

Large enhancement of the anomalous Hall effect in Co/Pt multilayers sandwiched by MgO layers

S. L. Zhang, J. Teng, J. Y. Zhang, Y. Liu, J. W. Li et al.

Citation: *Appl. Phys. Lett.* **97**, 222504 (2010); doi: 10.1063/1.3522653

View online: <http://dx.doi.org/10.1063/1.3522653>

View Table of Contents: <http://apl.aip.org/resource/1/APPLAB/v97/i22>

Published by the [AIP Publishing LLC](#).

Additional information on Appl. Phys. Lett.

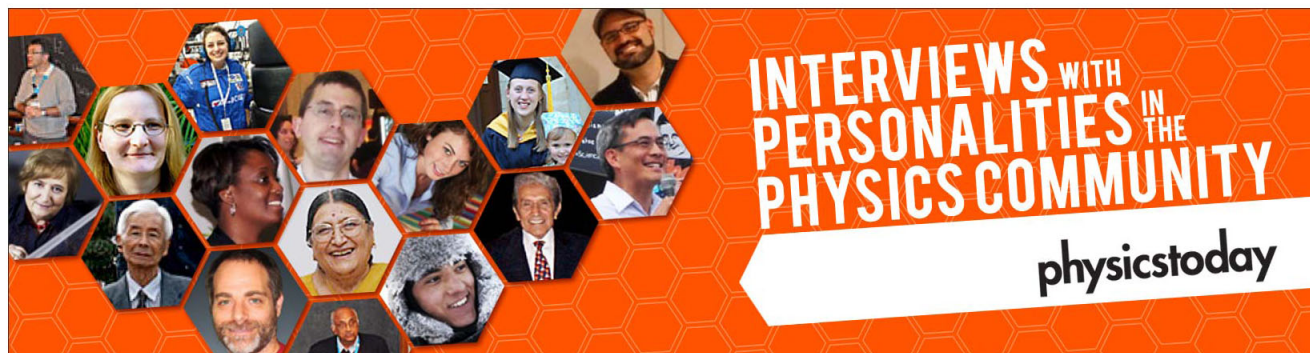
Journal Homepage: <http://apl.aip.org/>

Journal Information: http://apl.aip.org/about/about_the_journal

Top downloads: http://apl.aip.org/features/most_downloaded

Information for Authors: <http://apl.aip.org/authors>

ADVERTISEMENT



Large enhancement of the anomalous Hall effect in Co/Pt multilayers sandwiched by MgO layers

S. L. Zhang,¹ J. Teng,^{1,a)} J. Y. Zhang,¹ Y. Liu,¹ J. W. Li,¹ G. H. Yu,^{1,a)} and S. G. Wang²

¹Department of Materials Physics and Chemistry, University of Science and Technology Beijing, Beijing 100083, People's Republic of China

²State Key Laboratory of Magnetism, Institute of Physics, Chinese Academy of Sciences, Beijing 100190, People's Republic of China

(Received 15 September 2010; accepted 5 November 2010; published online 30 November 2010)

We report a large enhanced anomalous Hall effect (AHE) in the Co/Pt multilayers sandwiched by two MgO layers. The Hall resistivity (ρ_{xy}) was over an order of magnitude larger than that in pure Co/Pt multilayers. By optimizing the thickness of MgO layers, a high field sensitivity value of 2445 V/A T for Hall sensors was achieved. The enhancement of AHE is mainly attributed to the MgO–Pt interfacial effect. © 2010 American Institute of Physics. [doi:10.1063/1.3522653]

The anomalous Hall effect (AHE) has been extensively studied during the past few decades because of its controversial physical mechanism^{1–3} and its wide applications. Metallic materials with AHE have been used for magnetic sensors,^{4–6} showing some advantages over semiconductor Hall sensors, such as low resistivity, high operation frequency, and low temperature coefficient. For the AHE sensors, the field sensitivity is one of the primary parameters. A satisfactory sensitivity requires higher AHE resistivity (ρ_{xy}) and lower hard-axis saturation field (H_S). However, the materials with large ρ_{xy} exhibit high saturation field generally, while the ρ_{xy} in systems with low H_S is still of limited magnitudes so far. For example, large ρ_{xy} has been obtained in ϵ -Fe₃N nanocrystalline films⁷ which is over two orders of magnitude larger than that of bulk Fe, reaching about 20 $\mu\Omega$ cm. Unfortunately, its H_S is quite large (>10 kOe), suppressing the value of the sensitivity. Ultrathin CoFe/Pt multilayers have a low saturation field (~ 10 Oe), but its ρ_{xy} reaches only 0.6 $\mu\Omega$ cm,⁸ just the same level of the thin films of ordinary transition metals (~ 1 $\mu\Omega$ cm).⁹ Although the ρ_{xy} is not very large, the interface anisotropy in CoFe/Pt system allows for tuning the H_S and the linearity. The sensitivity could reach as high as 1200 V/A T, showing a competition with the best semiconductor Hall sensors.⁸ The multilayered system provides a promising chance for manipulating the anisotropy. Thus, the sensitivity can be substantially improved if ρ_{xy} in this system is greatly enhanced. Recent results have shown that the AHE can be amplified by enhancing the interfacial scattering, which is achieved by structural modifications. This idea was realized in the [Pt/Co]₅/Ru/[Co/Pt]₅ multilayers,¹⁰ where the AHE was much improved due to the strong Ru/Co interfacial scattering by introducing Ru spacer. Therefore, stimulating the interfacial scattering in multilayer systems is an encouraging approach for developing high-sensitivity AHE sensors.

Comparing with the metal-metal interface, the amorphous insulator-metal interface can increase the AHE more significantly because the amorphous insulator-metal interface contains more defects for additional scattering of electrons.¹¹ Recently, interfaces consisting of the insulator MgO are

shown to have a strong scattering capability for the tunnel magnetoresistance¹² and anisotropic magnetoresistance¹³ materials. In this paper, we report a method to enhance the AHE by introducing MgO (amorphous)-metal interfaces in the Co/Pt multilayers with tunable anisotropy for high-sensitivity Hall sensors.

Multilayered samples with structure of Pt(0.6)/[Co(0.4)/Pt(1.2)]_n (in nanometer) (pure Co/Pt multilayers, called S1), MgO($t_{\text{MgO}}^{\text{sub}}$)/Pt(0.6)/[Co(0.4)/Pt(1.2)]_m/MgO($t_{\text{MgO}}^{\text{top}}$) (in nanometer) (Co/Pt multilayers sandwiched

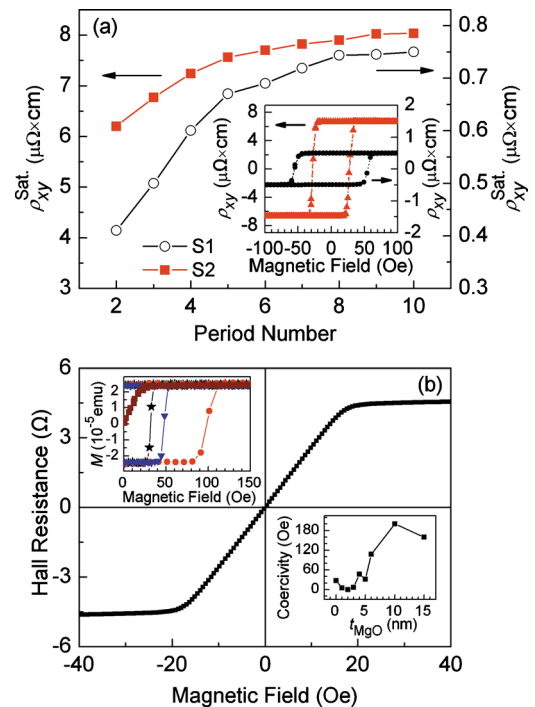


FIG. 1. (Color online) (a) Saturation Hall resistivity (ρ_{xy}^{sat}) as a function of period number n for S1 (empty circle) and ρ_{xy}^{sat} as a function of m for S2 ($t_{\text{MgO}}^{\text{sub}} = t_{\text{MgO}}^{\text{top}} = 5$ nm) (solid rectangle). Inset: Hall resistivity as a function of magnetic field measured at RT for multilayers $n=3$ (circle) and $m=3$, ($t_{\text{MgO}}^{\text{sub}} = t_{\text{MgO}}^{\text{top}} = 5$ nm) (triangle). (b) Hall resistance as a function of the field for the multilayer MgO(3)/Pt(0.6)/[Co(0.4)/Pt(1.2)]₃/MgO(1) (in nanometer). Right bottom inset: the coercivity as a function of t_{MgO} ($t_{\text{MgO}}^{\text{sub}} = t_{\text{MgO}}^{\text{top}}$) for S2, $m=3$. Left top inset: hysteresis loops for S2, $m=3$ with $t_{\text{MgO}}^{\text{sub}} = 3$ nm and varying $t_{\text{MgO}}^{\text{top}}$ (rectangle: $t_{\text{MgO}}^{\text{top}} = 1.5$ nm, star: $t_{\text{MgO}}^{\text{top}} = 2$ nm, triangle: $t_{\text{MgO}}^{\text{top}} = 3$ nm, and circle: $t_{\text{MgO}}^{\text{top}} = 4$ nm).

^{a)}Author to whom correspondence should be addressed. Electronic mail: ghyu@mater.ustb.edu.cn.

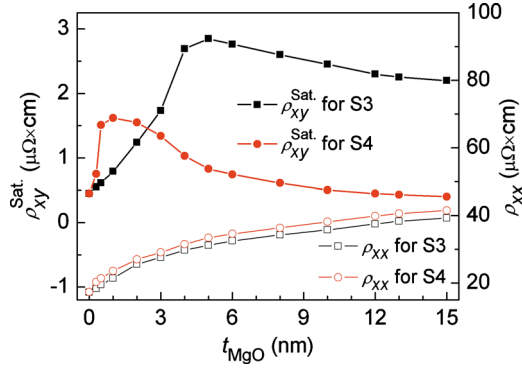


FIG. 2. (Color online) Saturation Hall resistivity ρ_{xy}^{sat} and longitudinal resistivity ρ_{xx} as a function of the MgO thickness for samples S3 and S4.

by MgO layers, called S2), $\text{MgO}(t_{\text{MgO}}^{\text{sub}})/\text{Pt}(0.6)/[\text{Co}(0.4)/\text{Pt}(1.2)]_3$ (in nanometer) (Co/Pt multilayers with MgO underneath, called S3), and $\text{Pt}(0.6)/[\text{Co}(0.4)/\text{Pt}(1.2)]_3/\text{MgO}(t_{\text{MgO}}^{\text{top}})$ (in nanometer) (Co/Pt multilayers with MgO on the top, called S4) were deposited onto thermally oxidized Si wafers at room temperature (RT) by magnetron sputtering. The thickness of the amorphous MgO layer ($t_{\text{MgO}}^{\text{sub}}$ and $t_{\text{MgO}}^{\text{top}}$) varies from 1 to 15 nm, and the period number (m and n) varies from 2 to 10, respectively. The base pressure was prior to 1.0×10^{-5} Pa, and the Ar pressure was kept at 0.2 Pa during sputtering. The deposition rate of Co, Pt, and MgO is 0.071, 0.068, and 0.005 nm/s, respectively. Standard optical photolithography was applied to fabricate the Hall bars for the transport measurement with physical property measurement system (produced by Quantum Design in USA) using the standard four-probe technique. Magnetic properties were also measured by alternating gradient magnetometer.

The inset of Fig. 1(a) shows the AHE resistivity as a function of the magnetic field measured at RT for multilayers of $\text{Pt}(0.6)/[\text{Co}(0.4)/\text{Pt}(1.2)]_3$ (in nanometer) (circle) and $\text{MgO}(5)/\text{Pt}(0.6)/[\text{Co}(0.4)/\text{Pt}(1.2)]_3/\text{MgO}(5)$ (in nanometer) (triangle). It shows that the Hall resistivity increases significantly when the pure Co/Pt multilayers are sandwiched by MgO layers. The saturation Hall resistivity (ρ_{xy}^{sat}) value reaches 6.7 $\mu\Omega \text{ cm}$, whereas it is only 0.5 $\mu\Omega \text{ cm}$ in the sample without MgO layers. The enhancement is approximately 13 times by introducing MgO layers on both sides. Furthermore, the period number of the Co/Pt bilayers ($n = m = 2 - 10$) slightly affects the magnitude of ρ_{xy}^{sat} both in S1 and S2, shown in Fig. 1(a), indicating that the enhancement of ρ_{xy} is due to the interfacial effect at the MgO–Pt interfaces instead of that at the Co–Pt interfaces in the multilayers. The right bottom inset of Fig. 1(b) shows the coercivity of the multilayers $\text{MgO}(t_{\text{MgO}})/\text{Pt}(0.6)/[\text{Co}(0.4)/\text{Pt}(1.2)]_3/\text{MgO}(t_{\text{MgO}})$ (in nanometer) as a function of t_{MgO} . It shows that the coercivity changes nonlinearly with the MgO thickness, suggesting a sensitive anisotropy in the multilayers. The left top inset shows the perpendicular hysteresis loops for the multilayers $\text{MgO}(t_{\text{MgO}}^{\text{sub}})/\text{Pt}(0.6)/[\text{Co}(0.4)/\text{Pt}(1.2)]_3/\text{MgO}(t_{\text{MgO}}^{\text{top}})$ (in nanometer) with $t_{\text{MgO}}^{\text{sub}} = 3$ nm and various $t_{\text{MgO}}^{\text{top}}$. For samples with $t_{\text{MgO}}^{\text{sub}}$ being around 3 nm and $t_{\text{MgO}}^{\text{top}}$ being around 1.5 nm, the magnetization loop shows an anisotropy shift from out-of-plane to in-plane. Thus, a high value of sensitivity with large ρ_{xy} and low hard-axis H_S can be obtained by optimizing the thicknesses of MgO layers. Figure 1(b) shows the Hall resistance loop at RT for the

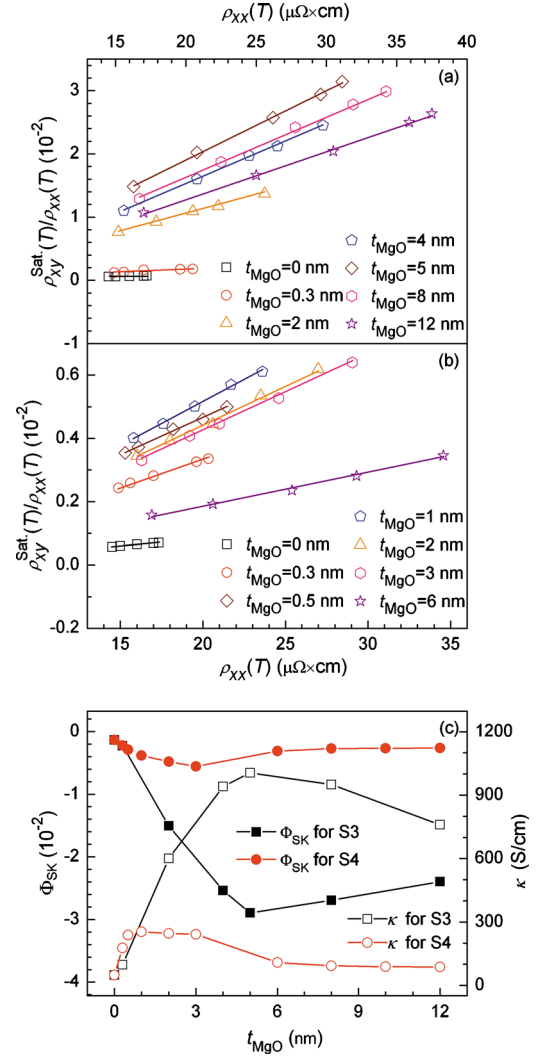


FIG. 3. (Color online) (a) $\rho_{xy}^{\text{sat}}(T)/\rho_{xx}(T)$ vs $\rho_{xx}(T)$ for S3 where each sample's $\rho_{xy}^{\text{sat}}(T)$ and $\rho_{xx}(T)$ were plotted in several different temperatures. (b) $\rho_{xy}^{\text{sat}}(T)/\rho_{xx}(T)$ vs $\rho_{xx}(T)$ for S4. (c) Φ_{SK} and κ as a function of the MgO thickness for S3 and S4.

sample $\text{MgO}(3)/\text{Pt}(0.6)/[\text{Co}(0.4)/\text{Pt}(1.2)]_3/\text{MgO}(1)$ (in nanometer). The Hall resistance is increased to 4.5 V/A, and the saturation field is only approximately 20 Oe. The Hall resistance loop shows a good linearity with field sensitivity as high as 2445 V/A T, which is about two times larger than that of the current best metallic Hall sensors (1200 V/A T).⁸

As the top and the bottom MgO layers have different influences on the interfacial crystalline morphology, it is necessary to investigate them, respectively. The focus is given on the two separated series of samples: S3 and S4. Figure 2 shows ρ_{xy}^{sat} and the longitudinal resistivity (ρ_{xx}) as a function of the thickness of MgO layer in S3 ($t_{\text{MgO}}^{\text{sub}}$) and S4 ($t_{\text{MgO}}^{\text{top}}$), respectively. The ρ_{xx} for both S3 and S4 shows a monotonic increase slightly with increasing the MgO thickness. The ρ_{xy}^{sat} increases significantly with increasing t_{MgO} for S3 and S4, with the maximum value at $t_{\text{MgO}}^{\text{sub}} = 5$ nm and $t_{\text{MgO}}^{\text{top}} = 2$ nm for S3 and S4, respectively. Then ρ_{xy}^{sat} decreases with further increasing t_{MgO} . For the optimized values of t_{MgO} in each series, ρ_{xy}^{sat} increases to 2.85 and 1.62 $\mu\Omega \text{ cm}$ compared with 0.5 $\mu\Omega \text{ cm}$ in multilayers without MgO layers. It shows six and three times larger in magnitude than that in the reference sample ($t_{\text{MgO}} = 0$ nm). It can be known by comparing S3 and

S4 that the top and the bottom MgO layers make different contributions to AHE. The highest value of ρ_{xy} is obtained in S2, indicating that the enhancement of the AHE is attributed to the interfacial effect at both the MgO/Pt and the Pt/MgO interfaces.

In general, the AHE has both intrinsic and extrinsic origins, and ρ_{xy}^{sat} can be expressed as

$$\rho_{xy}^{\text{sat}} = \Phi_{\text{sk}} \rho_{xx} + \kappa \rho_{xx}^2, \quad (1)$$

where the linear term with parameter Φ_{sk} stands for the extrinsic skew scattering¹⁴ and the parameter of the quadratic term κ incorporates two parts: one is the intrinsic conductivity κ^{int} which comes from the band structure effect,¹⁵ the other is the side-jump conductivity κ^{sj} which accumulates all the other extrinsic contributions to ρ_{xy}^{sat} ,¹⁶ and can be boosted by interface scattering usually in a multilayer system,¹⁷ i.e., $\kappa = \kappa^{\text{int}} + \kappa^{\text{sj}}$. Recently it is known from the work of Seemann *et al.*³ that the proportion of κ^{int} and κ^{sj} to κ is determined mainly by the spin-orbit coupling strength in the material. Often, Φ_{sk} and κ can be experimentally distinguished in a plot of $\rho_{xy}^{\text{sat}}/\rho_{xx}$ versus ρ_{xx} by varying ρ_{xy}^{sat} and ρ_{xx} through temperature changes.

Figures 3(a) and 3(b) show $\rho_{xy}^{\text{sat}}(T)/\rho_{xx}(T)$ versus $\rho_{xx}(T)$ for S3 and S4. Figure 3(c) shows the values of Φ_{sk} and κ derived from Figs. 3(a) and 3(b) as a function of t_{MgO} for samples S3 and S4. The maximum value of κ in S3 and S4 is about 21 and five times larger than that in pure Co/Pt multilayers, respectively. The larger κ is, the higher the AHE is. For Φ_{sk} , the maximum absolute value of Φ_{sk} is 25 and four times larger than those in pure Co/Pt multilayer for S3 and S4, respectively. However, the skew scattering contribution is always negative in our samples. Thus, the large enhanced AHE is dominated by the enhanced κ , which is determined by both κ^{sj} and κ^{int} . It is known that the scattering event contributes to both Φ_{sk} and κ , while the intrinsic origin only makes contribution to κ . Since the absolute values of Φ_{sk} and κ increase/decrease synchronously as t_{MgO} increases, indicating that the enhanced κ is not only due to the intrinsic mechanism, but also results from the scattering effect (side jump mechanism) at the MgO–Pt interface. This enhancement of κ can be mainly attributed to the MgO–Pt interfacial effect.

In conclusion, we have presented a detailed study of the AHE for Co/Pt multilayers sandwiched by two insulator amorphous MgO layers. The AHE for this multilayer is much larger than that of the system without MgO layers. By optimizing the thicknesses of MgO layers, an approach that enables generation of high-sensitivity AHE sensors is provided. The enhanced AHE in our multilayers is attributed to the large κ contribution, which is mainly due to the MgO–Pt interfacial effect.

This work is supported by the National High Technology Research and Development Program 863 (Grant No. 2007AA032310), the National Basic Research Program of China (Grant No. 2009CB929203), and the National Natural Science Foundation of China (Grant Nos. 51071023, 50871014, 50831002, 50901007, and 50972163).

¹Y. Tian, L. Ye, and X. Jin, *Phys. Rev. Lett.* **103**, 087206 (2009).

²E. Roman, Y. Mokrousov, and I. Souza, *Phys. Rev. Lett.* **103**, 097203 (2009).

³K. M. Seemann, Y. Mokrousov, A. Aziz, J. Miguel, F. Kronast, W. Kuch, M. G. Blamire, A. T. Hindmarch, B. J. Hickey, I. Souza, and C. H. Marrows, *Phys. Rev. Lett.* **104**, 076402 (2010).

⁴T. R. McGuire, R. J. Gambino, and R. C. Taylor, *J. Appl. Phys.* **48**, 2965 (1977).

⁵A. B. Pakhomov, X. Yan, and B. Zhao, *Appl. Phys. Lett.* **67**, 3497 (1995).

⁶G. X. Miao and G. Xiao, *Appl. Phys. Lett.* **85**, 73 (2004).

⁷Y. H. Cheng, R. K. Zheng, H. Liu, Y. Tian, and Z. Q. Li, *Phys. Rev. B* **80**, 174412 (2009).

⁸Y. Zhu and J. W. Cai, *Appl. Phys. Lett.* **90**, 012104 (2007).

⁹A. Gerber, A. Milner, M. Karpovsky, B. Lemke, H. U. Habermeier, J. Tuillon-Combes, M. Negrier, O. Boisson, P. Melinon, and A. Perez, *J. Magn. Magn. Mater.* **242–245**, 90 (2002).

¹⁰J. Zhao, Y. J. Wang, X. F. Han, S. Zhang, and X. H. Ma, *Phys. Rev. B* **81**, 172404 (2010).

¹¹N. Ryzhanova, A. Vedyayev, A. Pertsova, and B. Dieny, *Phys. Rev. B* **80**, 024410 (2009).

¹²A. Manchon, C. Ducruet, L. Lombard, S. Auffret, B. Rodmacq, B. Dieny, S. Pizzini, J. Vogel, V. Uhlir, M. Hochstrasser, and G. Panaccione, *J. Appl. Phys.* **104**, 043914 (2008).

¹³L. Ding, J. Teng, X. C. Wang, C. Feng, Y. Jiang, G. H. Yu, S. G. Wang, and R. C. C. Ward, *Appl. Phys. Lett.* **96**, 052515 (2010).

¹⁴J. Smit, *Physica* **24**, 39 (1958).

¹⁵R. Karplus and J. M. Luttinger, *Phys. Rev.* **95**, 1154 (1954).

¹⁶L. Berger, *Phys. Rev. B* **2**, 4559 (1970).

¹⁷C. L. Canedy, X. W. Li, and G. Xiao, *Phys. Rev. B* **62**, 508 (2000).